Available online at www.sciencedirect.com

SciVerse ScienceDirect

Journal of the European Ceramic Society 32 (2012) 753–764

www.elsevier.com/locate/jeurceramsoc

An overview of using solid wastes for pigment industry

W. Hajjaji [a,b,*], G. Costa [c], C. Zanelli [d], M.J. Ribeiro [c], M.P. Seabra [b], M. Dondi [d], J.A. Labrincha [b]

[a] *Geobiotec, Geosciences Dept., University of Aveiro, 3810-193 Aveiro, Portugal*
[b] *Ceramics and Glass Eng. Dept., CICECO, University of Aveiro, Aveiro, Portugal*
[c] *ESTG, Polytechnic Institute of Viana do Castelo, Viana do Castelo, Portugal*
[d] *Istituto di Scienza e Tecnologia dei Materiali Ceramici, CNR-ISTEC, 48018 Faenza, Italy*

Received 24 May 2011; received in revised form 4 October 2011; accepted 16 October 2011
Available online 6 November 2011

Abstract

This work reports the use of wastes (Al-rich anodizing sludge, Cr/Ni galvanizing sludge, foundry sand, tionite and marble sawing mud) to formulate distinct inorganic pigment structures that were synthesized by the solid state reaction method. One of the tested formulations is a novel pigment based on hibonite ($CaO{\cdot}6Al_2O_3$), that was found a suitable hosting structure to accommodate cobalt or nickel chromophore ions in tetrahedral coordination, then giving strong blue or turquoise hues, respectively. The use of Cr as chromophore was tested in three distinct pigment structures: (i) red-wine Cr–$CaSnSiO_5$ and brown Cr–$CaTiSiO_5$; (ii) Cr–$CaTiO_3$; (iii) and Cr–TiO_2. Developed phases were determined, and the colouring mechanisms of the chromophore species were defined based on diffuse reflectance data. Then, the pigments were added to a standard transparent glaze, and the hues which developed were estimated from *L*a*b** colorimetric measurements under the oxygen partial pressure in the atmosphere, to define stable workability window.

Keywords: Chromophore; Wastes; Ceramic pigments; Chromatic stability

1. Introduction

The growing ceramic materials market and the competitiveness of this sector constantly pushes manufacturers and researchers to find solutions to reduce the raw materials cost and, at the same time, to develop new formulations. Particular interest is given to the recycling of industrial wastes and natural sub-products, following the current trend in the search for alternative and less-expensive raw materials.[1] Industrial practices such as Al-anodizing,[2] Ni/Cr galvanizing,[3] marble sawing,[4] titania synthesis[5] and foundries[6] yield high amounts of sludge, that have to be treated and stored. Traditionally, such waste products are disposed of as soil conditioners or in land fill.[7,8]

Environment-friendly methods of producing new ceramic pigments obtained by solid state reaction from powdered mixtures of several industrial wastes were investigated. In the pigment, these by-products might act as host matrix or as a chromophore, depending on their chemical composition, particularly the nature and content of transition metal-ions. For the sake of comparison, each pigment formulation was also synthesized from chemically pure reagents, to assess variations in the required firing schedule and on the resulting colour. In fact, the normal production of pigments uses commercial chemicals that result from primary sources, but the use of secondary raw materials can also be attempted, if the resulting powders develop the desirable phases, and if their chromatic quality and stability on further application (namely as ceramic glazes) is retained. This solution should involve both economical and environmental benefits.

One of three hosting structures evolved in this work was hibonite doped with cobalt or nickel. This calcium hexaluminate ($CaAl_{12}O_{19}$ or $CaO{\cdot}6A_2O_3$) has a magnetoplumbite-type structure ($A^{[12]}M1^{[6]}M2^{[5]}M3_2{}^{[4]}M4_2{}^{[6]}M5_6{}^{[6]}O_{19}$) in which Al^{3+} ions are distributed over five different coordination sites, including three distinct octahedra (M1, M4 and M5), one tetrahedron (M3) and an unusual trigonal bipyramid (M2).[9,10] This framework allows a preferential partial substitution of the Al^{3+} ions by M^{2+} ions more effective at the M3 site.[10]

* Corresponding author at: Geobiotec, Geosciences Dept., University of Aveiro, 3810-193 Aveiro, Portugal. Tel.: +351 234370250; fax: +351 234370204.
E-mail address: w.hajjaji@ua.pt (W. Hajjaji).

0955-2219/$ – see front matter © 2011 Elsevier Ltd. All rights reserved.
doi:10.1016/j.jeurceramsoc.2011.10.018

The chromium was used in tin (malayaite) or titanium (titanite) sphenes. Also, Cr-doped perovskite and rutile was synthesized. The sphene structure is organized as parallel chains formed by corner-sharing MO_6-octahedra (M = Ti, Sn). These are linked to CaO_7-polyhedra via SiO_4-tetrahedra. O(2), O(3), O(4) and O(5) sites are occupied by oxygen atoms bound to the Si(IV) in tetrahedral coordination, while the O(1) site is linked to the M^{4+} cation.[11] The structural flexibility of this mineral group allows malayaite and titanite to have a large variety of atomic substitutions like Sn^{4+}, Ti^{4+} and Si^{4+} by chromium.[12,13] The same flexibility is permitted by rutile and perovskite corner-sharing frameworks and in situ distortions.[14,15]

2. Materials and methods

Distinct industrial wastes were used in this work: (i) sludges generated in the wastewater treatment of several activities: Al-anodizing (AS), marble sawing (MS), Cr/Ni plating (GS), and TiO_2 manufacturing (T); (ii) exhausted foundry sand from iron-casting processes (FS). Safety data and toxicity assessment are available for these wastes.[16,17] According to their chemical composition, assessed by X-ray fluorescence (XRF, Philips X'UNIQUE II), they replace one or more primary raw sources of alumina, calcite, chromium/nickel, titanium, and silica, respectively. Table 1 expresses the wastes average chemical composition, estimated from a minimum of five determinations of representative samples collected, in distinct moments, at the industrial units. This table also gives the composition and the commercial origin of the pure reagents used. As, T and GS wastes contain a significant amount of sulphur that is not a limitation because it is expected to act as a mineraliser and pigment industry is equipped to clean flue gas from kilns to prevent air pollution.[18,19] Moreover, in the normal production of pigments, the fired materials are commonly "washed" in order to leach out the non-fixed hazardous species and let their concentrations below the limit of toxicity defined according to standards. In Europe, the leaching tests are performed according to DIN 38414-S4 standard. This test was a priority and was used on formulations where the concentration of hazardous species is relatively high (e.g. black pigments).[16] However, the preparation of pigments and the firing conditions (if well adjusted) should contribute to immobilize the hazardous species into the structure and neutralize their harmful effects. Moreover, the addition to the applications such as glazes in relatively low amounts (only 5 wt.% pigment is added) also minimize the risks by diluting the hazardous species potentially non immobilized. Also, the resistant framework of the fired glaze matrix should contribute to retain and condemn the escape of toxic species.

Pigment formulations and the chosen codes are presented in Table 2. For each family, pure reagent based materials are designated as (P) and waste based as (W). In order to obtain fine and homogeneous slurries, the mixtures were wet ball-milled with water for 1 h, then dried at 110 °C and fired at an adequate temperature (also given in Table 2). The firing cycle was kept constant (3 h dwell time and heating/cooling rates of 5 °C/min.). The obtained powders were manually disintegrated and sieved to 63 μm. X-ray diffraction (XRD, Rigaku Geigerflex

Table 1
Chemical composition of the used raw materials (determined by XRF or given by the supplier) (in wt.%).

	Alumina (Alcoa CT 3000)	AS	Calcite (Calcitec M1)	MS	Silica (Sibelco P5000)	FS	Cobalt oxide (Panreac)	Cassiterite (CCT MP 889)	Titania (Kronos)	T	Ni(II) acetate (Riedel)	Cr(III) nitrate (Fluka)	GS
Al_2O_3	98.7	35.3	0.10	0.14	0.10	0.20	–	–	–	3.44	–	–	4.73
SiO_2	0.20	1.19	0.10	0.64	99.0	97.7	–	–	–	28.2	–	–	0.17
Fe_2O_3	0.37	1.41	0.07	0.24	0.06	1.12	–	–	0.03	2.05	–	–	1.57
CaO	0.10	2.99	55.6	55.5	0.10	0.20	–	–	–	3.33	–	–	19.5
Na_2O	0.01	0.35	0.01	–	0.05	–	–	–	–	–	–		3.42
K_2O	0.04	0.07	0.01	0.11	0.10	0.26	–	–	–	0.40	–	–	0.19
MgO	0.01	0.34	0.22	0.31	0.07	–	–	–	–	2.18	–	–	1.02
TiO_2	0.06	–	0.01	0.02	0.01	0.20	–	–	99.3	45.6	–	–	–
SnO_2	–	–	–	–	–	–	–	99.9	–	–	–	–	–
Co_3O_4	–	–	–	–	–	–	99.9	–	–	–	–	–	–
Cr_2O_3	–	–	–	–	–	0.20	–	–	–	0.05	–	37.50	12.8
NiO										–	30.0	–	17.4
SO_3	–	16.7	–	–	–	–	–	–	0.02	14.38	–	–	10.6
P_2O_5	–	–	–	–	–	–	–	–	0.02	–	–	–	8.75
LOI	0.50	40.0	43.9	43.0	0.50	0.20	–	–	0.10	–	–	–	20.7

Table 2
Components, samples reference and calcination temperature of the prepared pigments (P: pure reagents; W: waste based).

Structure	Pigment code	T (°C)	Alumina (Alcoa CT 3000)	AS	Calcite (Calcitec M1)	MS	Silica (Sibelco P 5000)	FS	Cobalt oxide (Panreac)	Cassiterite (CCT MP 989)	Titania (Kronos)	T	Ni(II) acetate (Riedel)	Cr(III) nitrate (Fluka)	GS
Hibonite	P-Hb–Co	1350	65.0	–	19.0	–	11.4	–	2.3	–	2.3	–	–	–	–
	W-Hb–Co	1350	–	80.8	–	13.0	–	4.2	1.0	–	1.0	–	–	–	–
	P-Hb–Ni	1400	61.8	–	17.7	–	10.6	–	–	–	2.1	–	7.7	–	–
	W-Hb–Ni	1400	–	76.3	–	12.0	–	3.9	–	–	0.9	–	6.9	–	–
Sphene	P-Tt	1450	–	–	39.4	–	23.6	–	–	–	30.1	–	–	6.9	–
	W-Tt	1450	–	–	–	35.2	–	25.1	–	–	31.9	–	–	–	7.8
	P-Ml	1300	–	–	31.1	–	18.8	–	–	45.5	–	–	–	4.4	–
	W-Ml	1300	–	–	–	28.4	–	6.1	–	45.9	–	–	–	–	19.6
Perovskite	P-Pv	1200	–	–	55.6	–	–	–	–	–	42.7	–	–	1.7	–
	W-Pv	1200	–	–	–	40.1	–	–	–	–	–	53.5	–	–	6.4
Rutile	P-Ru	1200	–	–	–	–	–	–	–	–	96.2	–	–	3.8	–
	W-Ru	1200		–	–	–	–	–	–	–	–	92.7	–	–	7.3

Table 3
Rietveld quantification of the prepared pigments (P: pure reagents; W: waste based). The agreement patterns: $17.3\% < R_{wp} < 27.3\%$, $13.1\% < R_p < 20.4\%$, $2.2 < \chi^2 < 5.9$, and $8.9\% < R(F2) < 25.2\%$.

Structure	Pigment code	T (°C)	Hibonite	Malayaite	Titanite	Perovskite	Rutile	Corundum	Anorthite	Gehlenite	Casseterite	Cristobalite	Wollastonite	Akermanite	Armalcolite	Nichromite	Nickel titanate	Anhydrite	Larnite
Hibonite	P-Hb–Co	1350	65.1	–	–	–	–	6.9	28.0	–	–	–	–	–	–	–	–	–	–
	W-Hb–Co	1350	75.6	–	–	–	–	2.9	–	21.5	–	–	–	–	–	–	–	–	–
	P-Hb–Ni	1400	69.4	–	–	–	–	4.1	26.5	–	–	–	–	–	–	–	–	–	–
	W-Hb–Ni	1400	88.3	–	–	–	–	6.7	–	5.0	–	–	–	–	–	–	–	–	–
Sphene	P-Tt	1450	–	–	98.7	1.3	–	–	–	–	–	–	–	–	–	–	–	–	–
	W-Tt	1450	–	–	90.2	–	–	–	–	–	–	5.0	–	–	–	–	4.7	–	–
	P-Ml	1300	–	97.1	–	–	–	–	–	–	2.1	–	–	–	–	–	–	–	–
	W-Ml	1300	–	85.8	–	–	–	–	–	–	12.1	1.5	–	–	–	5.5	–	–	–
Perovskite	P-Pv	1200	–	–	–	100	–	–	–	–	–	–	–	–	–	–	–	–	–
	W-Pv	1200	–	–	–	64.2	–	–	–	–	–	–	4.2	22.1	–	–	–	7.7	1.8
Rutile	P-Ru	1200	–	–	–	–	100	–	–	–	–	–	–	–	–	–	–	–	–
	W-Ru	1200	–	–	26.1	–	44.3	8.6	–	–	–	0.9	–	–	20.1	–	–	–	–

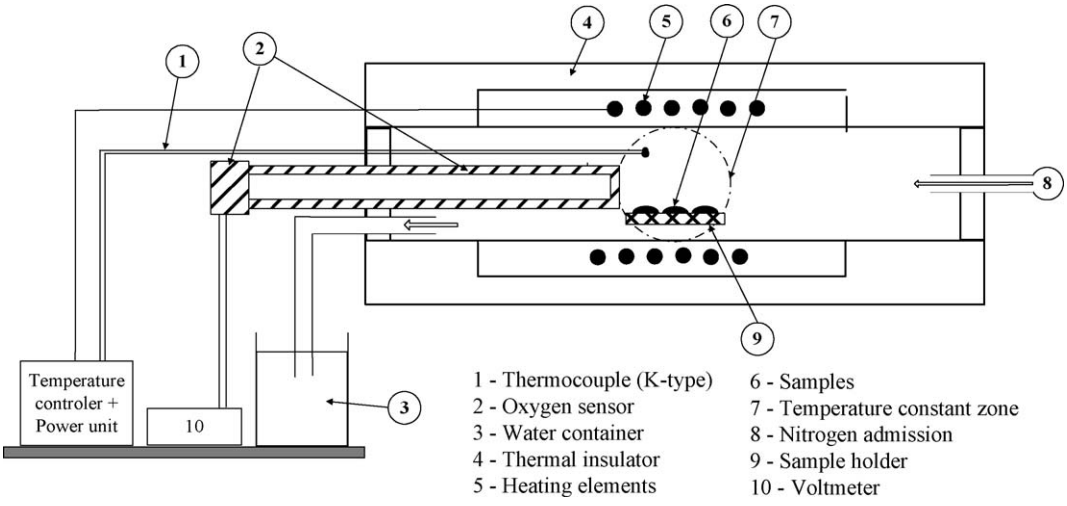

Fig. 1. Schematic view of firing furnace prepared for the oxygen partial pressure atmosphere control.

D/max – Series under the following conditions: CuKα radiation in the 10–80° 2θ range, scan rate 0.02° 2θ, 185 s equivalent per step) was carried out to identify the crystalline phases. The quantitative phase analysis was performed using GSAS-EXPGUI software following RIR (reference intensity ratio) and Rietveld refinement techniques.[20–22] Each X-ray powder diffraction pattern consists of approximately 5500 data points and 400 reflections. Up to 40 independent variables were refined: phase fractions, zero point, 15–20 coefficients of the shifted Chebyschev function to fit the background, unit cell parameters, profile coefficients (one Gaussian, Gw, and one Lorentzian term, Lx). The experimental uncertainty of phase amount quantification is 5%.

The colour was measured by absorption spectroscopy (Shimadzu UV-3100 UV–Vis–NIR), and by determining the *L*a*b** chromatic coordinates on a Konica Minolta Chroma Meter CR-400, using D65 illuminant and 10° standard observer.

Finally, each pigment was added (5 wt.%) to a commercial transparent bright ceramic glaze (60–65% SiO_2, 9–11% Al_2O_3, 14–17% B_2O_3, 3–5% CaO, 4–7% Na_2O, and 1% K_2O). Pellets (2.5 cm diameter) were pressed and then fired at 1050 °C for 30 min in an electric furnace. The *L*a*b** colorimetric values of the coloured glazes were evaluated and no formation of surface defects (bubbles, cracks, colour heterogeneities) was observed. The chromatic stability of the coloured glazes was studied, within certain limits, as a function of the oxygen partial pressure (pO_2) of the firing atmosphere. To perform these tests, a special sample holder was designed (Fig. 1), where the reduced atmospheres were obtained by controlling the nitrogen pressure admission (using the manual valve control). In order to ensure there was no parasitic air entrance into the furnace atmosphere, the exhaust nitrogen–air mixture was put under pressure by immersing the exit tube in a water container. The oxygen partial pressure (pO_2) was controlled using a voltmeter.

3. Results and discussion

3.1. Hibonite based pigments

In the hibonite structure, cobalt and nickel ions, in the co-presence of titanium (to assure their electroneutrality), were separately added, in an attempt to get strong blue (with Co) and turquoise (with Ni) hues[23,24] with the following stoichiometry, respectively:

- $Ca(Al_{11.7}Co_{0.03})O_{19}$; cobalt doped hibonite,
- $Ca(Al_{11.7}Ni_{0.03})O_{19}$; nickel doped hibonite.

Fig. 2 and Table 3 presents the XRD patterns and phase quantification of powders calcined between 1350 and 1400 °C, obtained from pure reagents (P-Hb–Co and P-Hb–Ni) or from industrial wastes (W-Hb–Co and W-Hb–Ni). In all cases, hibonite was identified as the major crystalline phase (65.1–88.3%), the higher percentages being in the waste based pigments; a clear argument for the wastes fluxing action. However, the secondary phase is different when pure or secondary raw materials are used. In the first case, the formation of anorthite occurs as predicted from the initial formulation, as can be seen in Fig. 3. By using wastes (W-pigments), instead of anorthite, gehlenite is detected. Residual corundum phase (2.9–6.9%) is also present in both cases, meaning that the reaction was not complete.[23,24] The presence of gehlenite in the waste based pigments is due to the wastes compositional complexity. The positioning of the prepared formulations on the $CaO–Al_2O_3–SiO_2$ ternary diagram (see Fig. 3)[25] explains this change. However, the chromatic characteristics of the pigments are not affected by that change, since both calcium aluminium silicates (anorthite and gehlenite) are mostly acting as fluxing or mineralising phases, helping to reduce the temperature of hibonite formation.

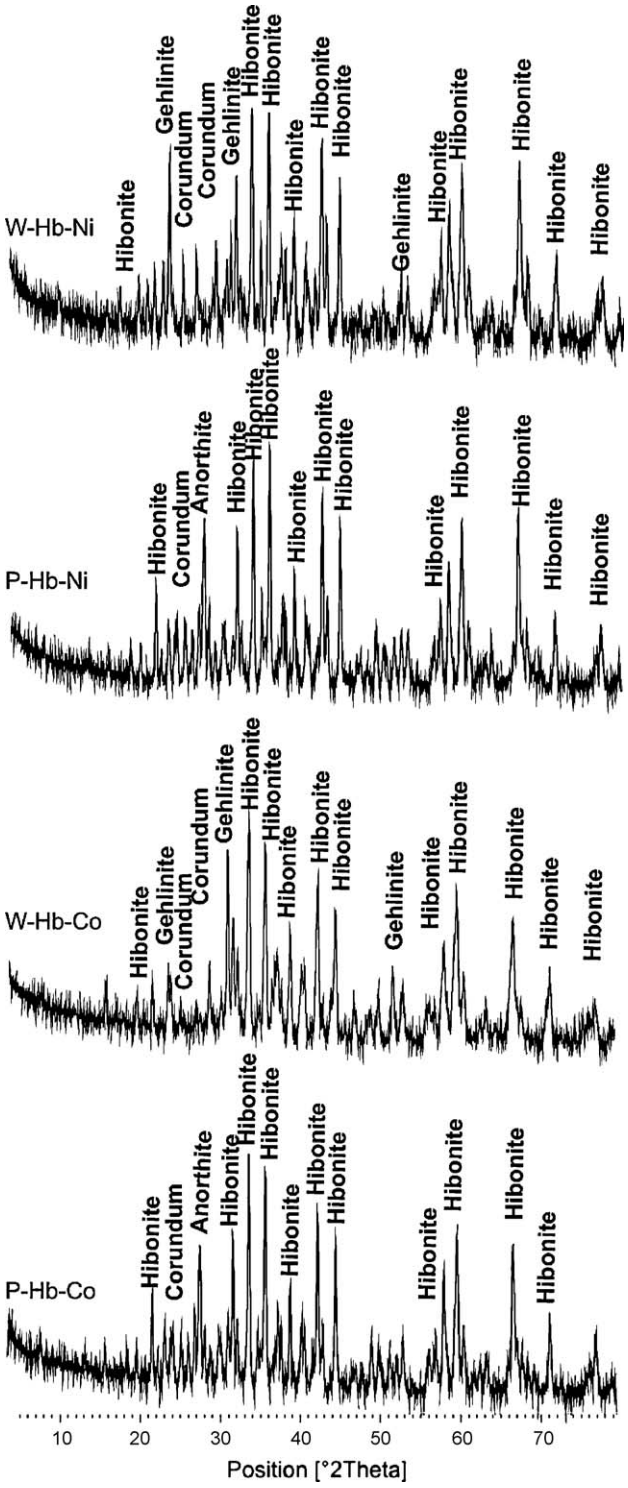

Fig. 2. XRD patterns of hibonite-based pigments.

On Hb–Co pigments the $-b^*$ chromatic coordinate is dominant, and L^* values are relatively low (Fig. 4 and Table 4). On Hb–Ni formulations $-a^*$ and $-b^*$ values are close, and L^* is higher, as expected for a bright turquoise hue. In both cases, the chromophore species (Co^{2+} or Ni^{2+}) is in a tetrahedral position (M3 site) on the hibonite lattice. This conclusion is supported by the optical spectra (Fig. 5). Three intense absorption bands were detected in the 540–650 nm range, which are associated with the $^4A_2(F) \rightarrow {}^4T_1(P)$ forbidden d–d transitions of Co^{2+} ($3d^7$) ions[23,26,27] and spin-allowed transitions of Ni^{2+} ($3d^8$), from the ground state $^3T_1$ (^3F) to $^3T_1$ (^3P), when they are in a tetrahedral field (T_d).[24,28]

The powders processed from pure reagents (P-pigments) present a slightly higher value of blue component ($-b^*$) than those obtained from wastes (W-pigments). This difference was also visible when pigments were added to colour the transparent and bright glazes (see Fig. 4 and Table 4). Hibonite is not stable in the glaze under current investigation conditions and it acts as a dye: cobalt even dissolved in the glassy phase developed strong and stable hues,[29] while the turquoise blue of Ni-containing pigments is lost (b^* is no longer negative) because Ni^{2+} in glassy phase moves to octahedral coordination, as attested by the presence of the exited state $^3A_2(F)$ (Fig. 5).[30] In fact, b^* values of the glaze coloured by Hb–Co pigments stayed close to −20, and not very far way from the values given by the pigments. The use of wastes lead to a slight decrease of the blue component, the colouring power is no worse than that of the P-Hb–Co pigment.

$L^*a^*b^*$ values of coloured glazes heat treated at 1050 °C in atmospheres having distinct O_2 contents (21%, 10–5% and 2–0.1%O_2) are given in Table 4. Integrated colour changes are normally given by the equation $\Delta E^* = [(\Delta L^*)^2 + (\Delta a^*)^2 + (\Delta b^*)^2]^{1/2}$ (the colour is indistinguishable for $\Delta E^* < 1$), and this parameter was calculated assuming, as reference, the normal air atmosphere (21% O_2). The coloured glazes fired in a reducing atmosphere (10–5% O_2) reveal chromatic stability ($\Delta E^* < 0.67$, Table 4). Only in very reducing conditions (2–0.1% O_2), at least when compared with that predictably achievable with common industrial firing conditions, does the colour tend to change. However, the maximum ΔE^* are below 2.51 and 4.34, respectively, for transparent glazes coloured with P-Hb and W-Hb pigments, the changes being mostly caused by the L^* parameter alteration.

3.2. Sphene based pigments

As mentioned before, Cr ions were explored here as chromophore elements in distinct pigment structures. As secondary raw source of Cr Cr/Ni plating sludges were used, aiming also to evaluate if the co-presence of nickel generates unwelcome colour changes. Cr-doped Malayaite [$Ca(Sn,Cr)SiO_5$] and titanite [$Ca(Ti,Cr)SiO_5$] sphenes were the two selected structures, as attempted to get, respectively, wine-red and brown stable pigments[31,32] with the following stoichiometry, respectively:

- $Ca(Sn_{0.96}Cr_{0.04})SiO_5$; Cr-doped malayaite,
- $Ca(Ti_{0.96}Cr_{0.04})SiO_5$; Cr-doped titanite.

In the synthesis of titanite from commercial reagents generates, after calcination at 1450 °C, 98.7% is the desired phase (Table 3). In the other case, after calcination at 1300 °C, malayaite (97.1%) is associated with cassiterite (2.1%), denoting that reaction was not completed [31]. The occurrence of this secondary phase is even more apparent in W-Ml formulations which contain 12.1% cassiterite (Fig. 6 and Table 3). Moreover,

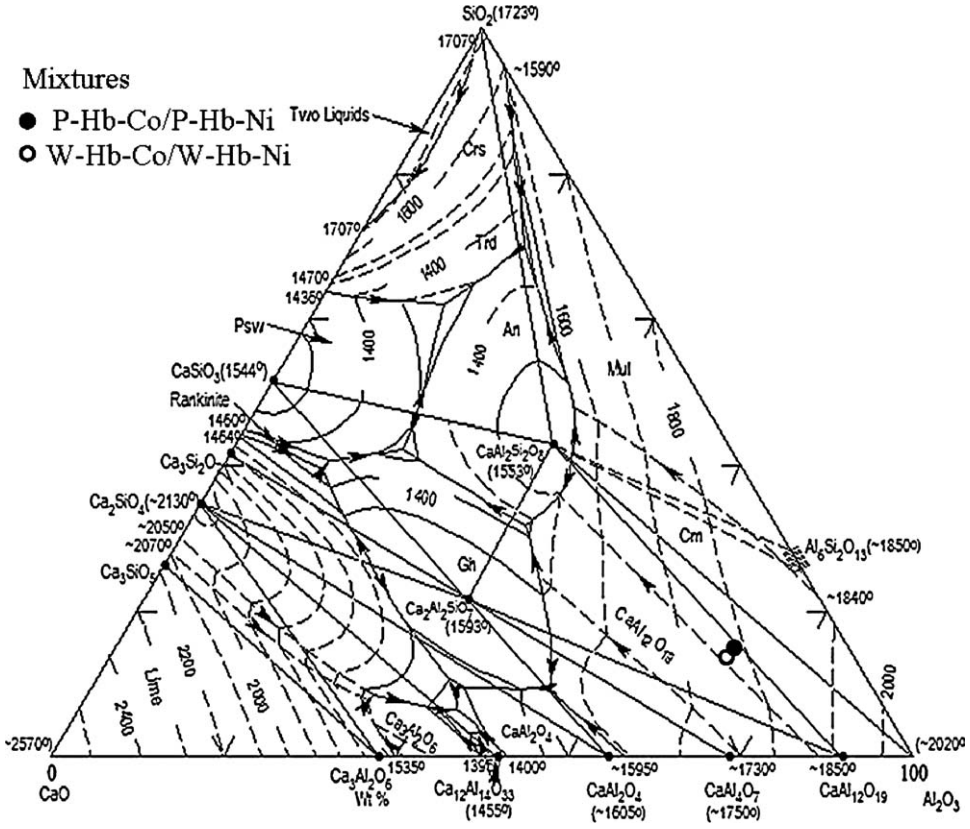

Fig. 3. $CaO–Al_2O_3–SiO_2$ ternary diagram [21].

the use of wastes in the pigments' formulation led to the formation of extra phases, namely, nickel titanate ($NiTiO_3$) and nichromite ($NiCr_2O_4$) in W-Tt and W-Ml, respectively. Cristobalite (SiO_2) was also detected in both waste based formulations. As suggested by the analysis of the relevant ternary diagram (Fig. 7),[33–35] the nickel should be assimilated by perovskite and spinel compounds, replacing calcium ions that are consumed in the sphene structure formation.

As shown in Fig. 4 and then confirmed by colorimetric measurements (Table 4), brown and wine-red hues were obtained for titanite and malayaite pigments, respectively. Colour differences between P- and W-pigments are stronger in the case of titanite and are emphasized when colouring the transparent glaze. Red-wine Cr–malayaite produces interesting red colours $a^* = 14.8$ (P sample) and $a^* = 16$ (W sample using inert wastes MS and FS). For brown Cr–titanite produces $a^* = 7.5$ (acceptable) for P sample but in W waste sample greenish ($a^* = -0.5$) indicating that pigment is slightly unstable. At the same scale, the glazes coloured with waste based pigments exhibit higher b^* values than those coloured with P-pigments. This behaviour can denote the occurrence of a reaction between some wastes' impurities (e.g. Ni, Fe) and the glaze. Nevertheless, the general chromatic development, in both structures, is governed by the chromium electronic configuration in the major hosting phase. Fig. 5 shows the optical spectra of Ml and Tt pigments. Titanite presents two clear absorbance bands: (i) the first one, at 405 nm, is attributed to the $^3A_2 \rightarrow {}^3T_2(P)$ transition of Cr(IV) species[32,36]; (ii) the second, located at around 500 nm, matches the spin-allowed transition of octahedral Cr^{3+} ions from $^4A_{2g}$ ground state to the excited $^4T_{1g}(F)$ state.[36] In the same optical interval, the spectrum of malayaite based pigment shows a band (at 505 nm) assigned to the $^4A_{2g} \rightarrow {}^4T_{2g}$ spin-allowed transition of Cr^{3+} ions in octahedral coordination.[13,14] Weaker peaks, that emerge between 600 and 750 nm, demonstrate the coexistence of octahedral Cr^{3+} in the cassiterite structure. The second wide band, positioned in the NIR zone, is assigned to the $^3A_2 \rightarrow {}^3T_1$ transition of Cr(IV) that is replacing tetrahedral Si^{4+}.[37,38]

The colour stability tests of glazes with the titanite pigments (P- and W-based) fired in atmospheres with distinct O_2 contents revealed an undesirable colour change from brown to green hues, for oxygen contents below 5%. This suggests a reduction of Cr(IV) to Cr(III) and its interaction with the glaze, and possibly release of chromium ions with the structure destruction of the synthesized titanite. L^* and a^* coordinates reached, respectively, 53.5 and −6.1 values denoting strong chromatic variations: $\Delta E^* \leq 11.35$ (P-Tt pigments) and $\Delta E^* \leq 7.06$ (W-Tt). By contrast, malayaite pigments are much more stable for the most reducing atmosphere (0.1–2% O_2), where $\Delta E^* \leq 3.71$ (Table 4).

3.3. Rutile and perovskite pigments

Two other families of brown pigments were studied in attempting to consume the hazardous tionite waste: $(Ca,Cr)TiO_3$

Fig. 4. Aspect of pigments and coloured glazes.

perovskite (P-Pv and W-Pv, when produced from pure reagents or by using wastes, respectively) and (Ti,Cr)O_2 rutile (P-Ru or W-Ru). Their formulations are given in Table 2, and the maximum firing temperature was 1200 °C:

- $Ca(Cr_{0.04}Ti_{0.96})O_3$; Cr-doped perovskite,
- $(Cr_{0.04}Ti_{0.96})O_2$; Cr-doped rutile.

P-Pv and P-Ru formulations developed the desirable single phases: perovskite and rutile, respectively (Fig. 8, Table 3). The corresponding counterparts prepared from wastes (T, GS and MS sludges) also show perovskite (64.2 wt.%) and rutile (44.3 wt.%) as major phases, as estimated by the Rietveld method from XRD spectra. However, the presence of impurities in the industrial wastes used (Si, Fe, Ni, etc.) lead to the

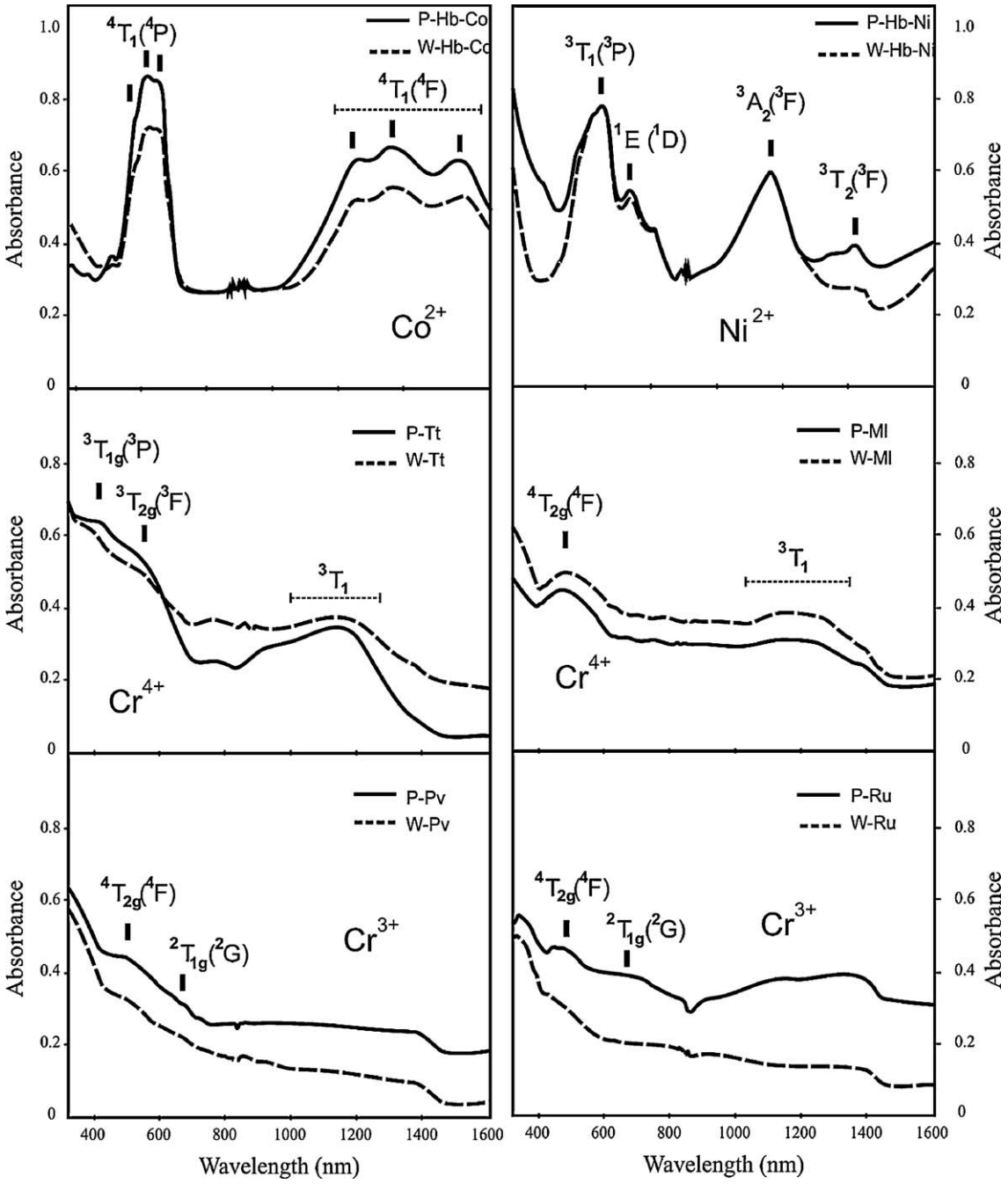

Fig. 5. Optical spectra of pigments: Hb = hibonite, Ti = titanite, Ml = malayaite, Pv = perovskite, Ru = rutile. The main electronic transitions are indicated for Co^{2+} and Ni^{2+} in tetrahedral coordination (hibonite); Cr^{4+} in both tetrahedral and octahedral coordination (titanite and malayaite); Cr^{3+} in octahedral coordination (perovskite and rutile).

formation of other phases. In W-Pv pigment, the abundance of silica (28.2 wt.%) in the tionite sludge causes the formation of calcium silicates, such as wollastonite ($CaSiO_3$), akermanite ($Ca_2MgSi_2O_7$; rankinite equivalent) and larnite (Ca_2SiO_4). P-Pv and W-Pv compositions were represented within the $CaO–TiO_2–SiO_2$ phase diagram,[33,35,39] belonging their composition to the $CaTiO_3–CaSiO_3–Ca_2SiO_4$ compatibility triangle (see Fig. 7). As Si replaces Ti in the perovskite structure to give wollastonite (in the W-Pv powder), there is a similar tendency for titanite ($CaTiSiO_5$) formation in the W-Ru pigment.[33,40] The relative calcium deficiency in tionite sludge (CaO/TiO_2 ratio is lower than in the stoichiometric P-Pv formulation) inhibited the formation of perovskite, and instead $CaTi_2O_5$ ($CaTiO_3 + TiO_2$) appeared. Nevertheless, the metastable character of this last compound, and the presence of Si, Mg, and Fe in the T sludge, supported the development of titanite and armalcolite $(Mg,Fe)Ti_2O_5$ (see Fig. 8).

The pigments' colour and the $L^*a^*b^*$ measured coordinates are shown in Fig. 4 and Table 4. The pure Cr-doped perovskite (P-Pv) exhibits higher red chroma ($a^* = 4.4$) than the W-Pv

Table 4
$L^*a^*b^*$ of the prepared pigments and coloured glazes at different pO_2 atmospheres (P: pure reagents; W: waste based).

Structure	Pigment code	Pigments			Transparent glaze										
					pO_2 21%			pO_2 10–5%				pO_2 2–0.1%			
		L^*	a^*	b^*	L^*	a^*	b^*	L^*	a^*	b^*	(((	L^*	a^*	b^*	(((
Hibonite	P-Hb–Co	56.8	2.6	−32.4	43.6	5.6	−18.4	43.8	6.1	−18.0	0.67	43.7	3.9	−17.1	2.16
	W-Hb–Co	61.5	−0.2	−26.7	47.5	4.2	−17.3	47.4	4.1	−17.8	0.52	43.9	5.6	−19.2	4.34
	P-Hb–Ni	73.3	−5.1	−8.7	53.7	−5.9	9.0	54.3	−6.0	9.2	0.64	56.2	−6	9.2	2.51
	W-Hb–Ni	68.2	−4.2	−7.9	66.0	−8.6	5.6	66.5	−8.2	5.6	0.64	69.6	−8.8	5.9	3.62
Sphene	P-Tt	56.8	3.1	12.5	46.1	7.5	19.2	47.0	7.3	19.9	1.16	48.7	−2.8	15.2	11.35
	W-Tt	54.8	0.0	10.2	49.7	−0.5	16.0	50.2	−0.7	15.3	0.88	53.5	−6.1	18.0	7.06
	P-Ml	42.7	18.9	4.6	43.2	14.8	7.5	43.9	14.5	7.6	0.77	39.6	13.9	7.5	3.71
	W-Ml	44.8	10.3	1.6	44.9	16	8.3	45.2	16.1	8.6	0.44	42.6	14.4	8.5	2.81
Perovskite	P-Pv	48.3	4.4	9.3	50.7	5.9	18.9	51.2	6.1	19.4	0.73	56.9	−10.8	15.4	18.19
	W-Pv	41.5	2.2	9.2	61.2	−2.5	15.5	61.7	−1.9	15.2	0.84	61.5	−5.0	18.4	3.88
Rutile	P-Ru	36.3	0.6	7.6	45.8	12.4	31.8	46.4	12.9	30.8	1.27	51.4	10.1	37.3	8.19
	W-Ru	40.1	2.0	10.5	56.2	4.6	32.1	57.1	4.8	32.5	1.00	56.8	2.0	35.3	4.12

Fig. 6. XRD patterns of titanite (Tt) and malayaite (Ml) pigments.

pigment ($a^* = 2.2$), but it is brighter (higher L^*). The absorbance spectrum of P-Pv powder shows a two main bands band at 505 and 640 nm in the visible region (see Fig. 5). These optical responses, less individualized in W-Pv, correspond to the spin-allowed and forbidden transitions of octahedral Cr^{3+} (d^3

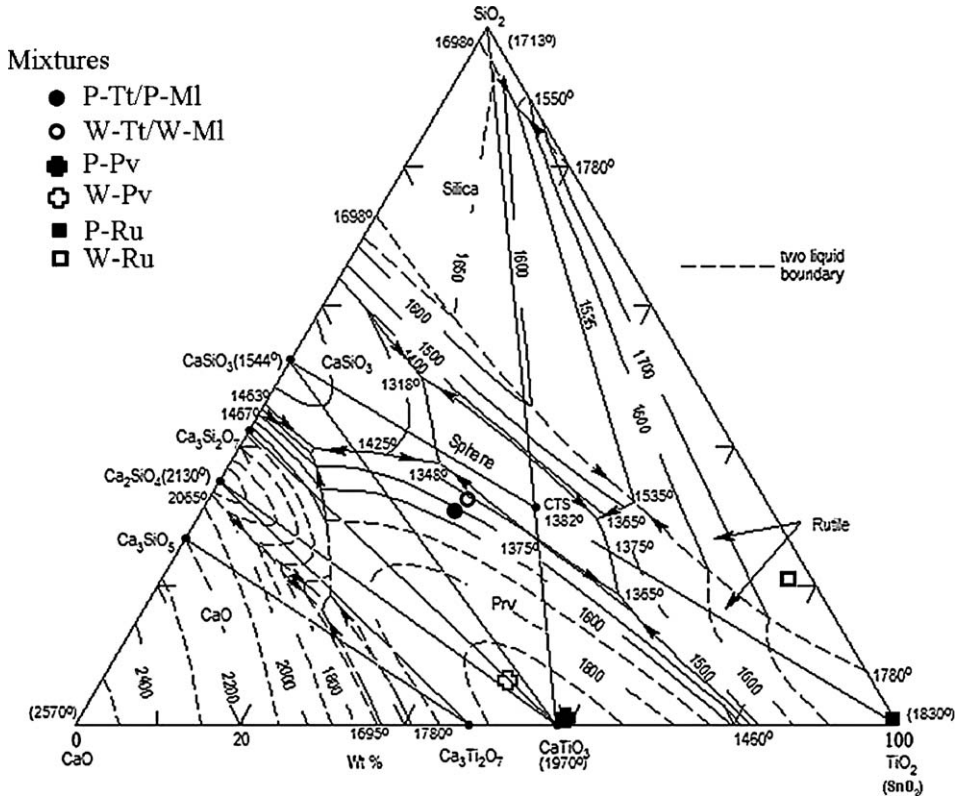

Fig. 7. CaO–TiO_2–SiO_2 ternary diagram (SnO_2 instead of TiO_2 in case of Ml).

electronic configuration) from $^4A_{2g}$ ground state to the excited $^4T_{1g}$(F) and $^2T_{1g}$(G) states.[41,42]

Chromium-doped rutile pigments show a dominant darker brown hue, as clearly seen in Fig. 4. When compared with P-Pv or W-Pv pigments, their brightness (L^*) is lower and the red chroma (+a*) in also smaller (Table 4). The compositional complexity of T and GS sludges affects the W-Ru pigment colour, that becomes brighter and shows higher a^* and b^* values than the P-Ru counterpart. This change is certainly related to the co-formation of titanite and armalcolite. The absorbance spectrum of rutile based pigments (P-Ru and W-Ru) is similar to those for perovskite based ones. The same the same pattern for the bands is visible (Fig. 5), which are attributed to the characteristic Cr^{3+} excitations υ_1 and υ_3 in the visible domain associated to $^4A_{2g} \rightarrow {}^4T_{2g}$(F) and $^4A_{2g} \rightarrow {}^2T_{1g}$(G) transitions.[42]

When used to colour the selected transparent glaze, the hue differences are also visible. Mainly the brown shade is different between P-Pv (pink brown) and P-Ru (orange brown) pigments (see Fig. 4 and Table 4). For red-brown Cr–perovskite,[41] this colour is obtained with 0.015 mole of Cr per unit formula and produces in monoporosa glaze $L^*a^*b^* = 45.2/15.3/5.3$. In the case of P sample ($a^* = 5.9$, $b^* = 18.9$) a light brown is obtained but W sample greenish ($a = -2.5$) and the pigment is not produced (see Table 4). By Fig. 4, the colour aspect developed by the W-Pv pigment in the glaze seems very similar to that of the pigment and more stable. Nevertheless, a slight difference is observed in $L^*a^*b^*$ measurements (see Table 4), especially with the increasing of the green component ($-a^*$). Cr–rutile pigments are normally obtained by codoping with A^{3+} = Cr, Fe and B^{5+} = Sb, Nb, W in order to preserve charge neutrality of the network, and starting from anatase as Ti precursor.[43] A brown colour is obtained in P ($a^* = 12.4$) sample that diminish to $a^* = 4.6$ in W sample. For the W-Ru pigment in the glaze, since the yellow component ($+b^*$) tends to increase (Table 4). In this pigment, the formation of extra phases determines the colour differentiation relative to P-Ru. Moreover, the presence of Fe-impurities in the wastes might also change the final colouration of the pigments, and further addition of chromium is required to improve their colouring power of the glazes.

Upon firing in reducing atmospheric conditions (2–0.1% O_2), the colour of glazes containing waste based pigments (W-Pv and W-Ru) remains much more stable than in the case of P-Pv and P-Ru counterparts (see Table 3). The maximum value of integrated chromatic variations (ΔE^*) of W-based pigments is 4.12. By contrast, ΔE^* reachs18.19 for the glaze coloured with the P-Pv pigment and fired in a very reducing atmosphere (%$O_2 < 2$). A green hue tends to be developed when the coloured glaze is fired in an extremely oxygen deficient atmosphere. In any case, it must be stressed that the colour changes, due to the O_2 content in the firing atmosphere, are only visible in very reducing conditions (%$O_2 < 2$), and it is somewhat unrealistic to expect this to occur in the current processing conditions of industrial ceramic production.

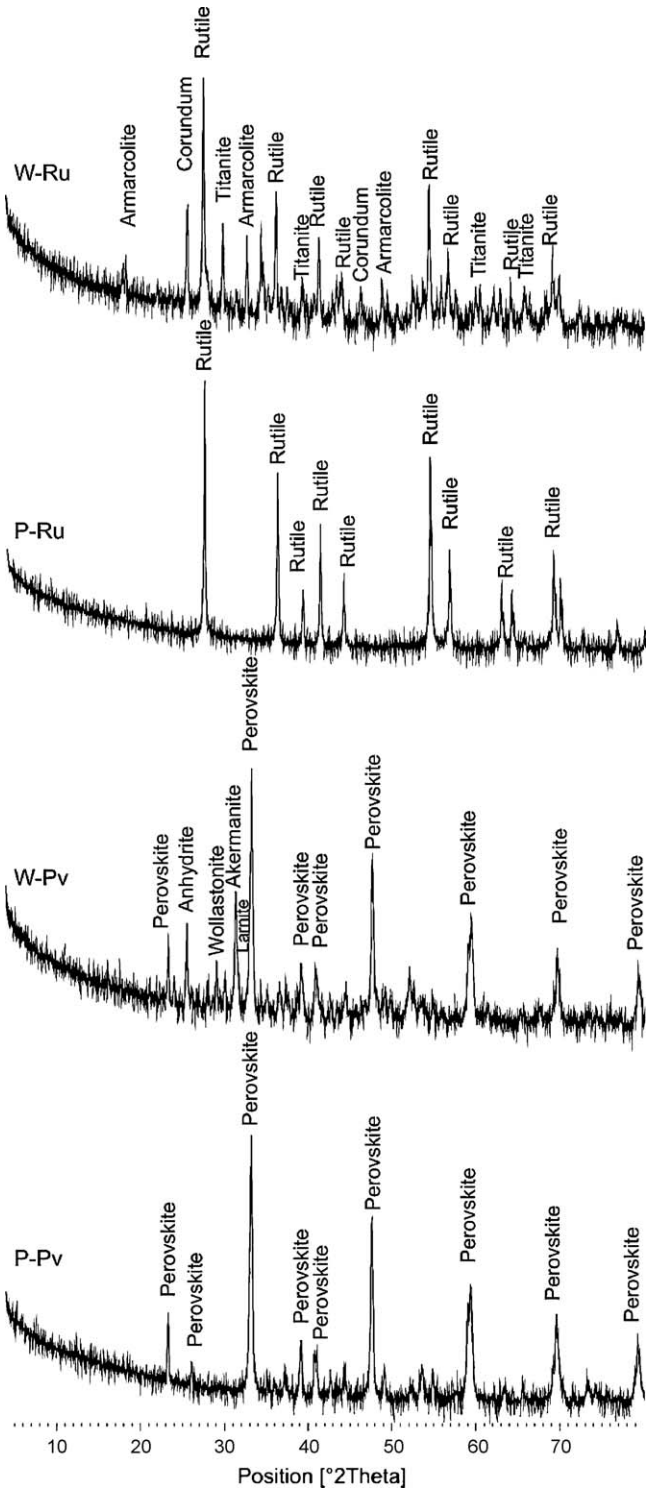

Fig. 8. XRD patterns of perovskite and rutile pigments.

4. Conclusions

The recycling of industrial sludges in ceramic pigment synthesis was tested in this work. For hibonite doped with cobalt or nickel, blue and turquoise colours were obtained. The incorporation of the chromophore elements Co^{2+} ($3d^7$) and Ni^{2+} ($3d^8$) was detected in a tetrahedral position (M3 site). When used for colouring transparent bright ceramic glazes, hibonite seems not stable in the glaze under current investigation conditions and it acts as a dye. Moreover, Ni^{2+} in glassy phase moves to octahedral coordination shading the final colour. For sphenes structures (malayaite and titanite), stable wine-red and brown pigments with a high colouring efficiency were obtained from industrial wastes. The substitution of tin or titanium by Cr(IV), in octahedral coordination, is the reason for the existence of these colours. In brown Cr–perovskite and maroon Cr–rutile pigments, Cr^{3+} was identified in the optical spectra by the main associated transition $^4A_{2g} \rightarrow {}^4T_{2g}$. This also demonstrated, in all cases, the mineraliser/stabilizer action of the impurities present in the sludges, and their contribution to the enhancement of the pigments' colouring efficiency and stability.

Acknowledgment

The work was supported by FCT (Project PTDC/CTM/72318/2006).

References

1. Hendriks F, Janssen GMT, Vázquez E. Use of Recycled Materials – Final Report of RILEM TC 198-URM; 2005.
2. Ribeiro MJ, Ferreira JMF, Labrincha JA. Extrusion of recycled pastes based on Al-rich anodising sludge. *Key Eng Mater* 2004;**2449**:264–8.
3. Ribeiro A, Hajjaji W, Seabra MP, Labrincha JA. Malayaite ceramic pigments prepared from industrial wastes: formulation and characterization. *J Mater Sci Forum* 2010;**636–637**:1371–6.
4. Montero MA, Jordán MM, Hernández-Crespo MS, Sanfeliu T. The use of sewage sludge and marble residues in the manufacture of ceramic tile bodies. *Appl Clay Sci* 2009;**46**:404–8.
5. Dondi M, Guarini G, Raimondo M, Zanelli C, Dalle Fabbriche D, Agostini A. Recycling the insoluble residue from titania slag dissolution (tionite) in clay bricks. *Ceram Int* 2010;**36**:2461–7.
6. Siddique R, Noumowe A. Utilization of spent foundry sand in controlled low-strength materials and concrete. *Conserv Recycling* 2008;**53**:27–35.
7. Cheremisinoff NP, Cheremisinoff PN. Hazardous materials and waste management. A Guide for the Professional Hazards Manager, William Andrew; 2005.
8. Williams PT. *Waste treatment and disposal*. 2nd ed. England: John Wiley & Sons; 2005.
9. Bermanec V, Holtstam D, Sturman D, Criddle AJ, Back ME, Šćaviničar S. Nežilovite, a new member of the magnetoplumbite group, and the crystal chemistry of magnetoplumbite group, and the crystal chemistry of magnetoplumbite and hibonite. *Can Mineral* 1996;**34**:1287–97.
10. Lin-Shu Du, Stebbins JF. Calcium and strontium hexaluminates: NMR evidence that "pentacoordinate" cation sites are four-coordinated. *J Phys Chem B* 2004;**108**:3681–5.
11. Kunz M, Xirouchakis D, Wang Y, Parise JB, Lindsley DH, Schweiz. Structural investigations along the join $CaTiOSiO_4$–$CaSnOSiO_4$. *Miner Petrog* 1997;**77**:1–11.
12. Heyns AM, Harden PM, Prinsloo LC. Resonance Raman study of the high-pressure phase transition in chromium-doped titanite. $CaTiOSiO_4$. *J Raman Spectrosc* 2000;**31**:837–41.
13. Lopez-Navarrete E, Caballero A, Orera VM, Lázaro FJ, Ocaña M. Oxidation state and localization of chromium ions in Cr-doped cassiterite and Cr-doped malayaite. *Acta Mater* 2003;**51**:2371–81.
14. Liu X, Liebermann RC. X-ray powder diffraction study of $CaTiO_3$ perovskite at high temperatures. *Phys Chem Miner* 1993;**20**:171–5.
15. Diebold U. The surface science of titanium dioxide. *Surf Sci Rep* 2003;**48**:53–229.

16. Costa MG. Valorização de resíduos industriais na formulação de produtos e pigmentos cerâmicos: Processamento e desenvolvimento de cor. PhD Thesis. Universidade de Aveiro 2009.
17. Dondi M, Zanelli C, Raimondo M, Guarini G, Dalle Fabbriche D, Agostini A. Recycling titania slag insolute residue ("Tionite") in clay bricks. *Ceram Int* 2010;**36**:2461–7.
18. World Bank Group in collaboration with the United Nations Environment Programme and the United Nations. Industrial Development Organization Pollution Prevention and Abatement Handbook; 1998.
19. Italian Ceramic Society, Colour, Pigments and Colouring in Ceramics. SALA, Modena; 2003.
20. Gualtieri AF. Accuracy of XRPD QPA using the combined Rietveld-RIR method. *J Appl Crystallogr* 2000;**33**:267–78.
21. Larson AC, Von Dreele RB. General structure analysis system (GSAS). Los Alamos National Laboratory, Report LAUR; 2000.
22. Toby BH. EXPGUI, a graphical user interface for GSAS. *J Appl Cryst* 2001;**34**:210–3.
23. Hajjaji W, Seabra MP, Labrincha JA. Recycling of solid wastes in the synthesis of Co-bearing calcium hexaluminate pigment. *Dyes Pigments* 2009;**83**:385–90.
24. Costa G, Ribeiro MJ, Hajjaji W, Seabra MP, Labrincha JA, Dondi M, et al. Ni-doped hibonite ($CaAl_{12}O_{19}$): a new turquoise blue ceramic pigment. *J Eur Ceram Soc* 2009;**29**:2671–8.
25. Gentile AL, Foster WR. Calcium hexaluminate and its stability relations in the system $CaO–Al_2O_3–SiO_2$. *J Am Ceram Soc* 1963;**46**:74–6.
26. Zayat M, Levy D. Blue $CoAl_2O_4$ particles prepared by the sol–gel and citrate–gel methods. *Chem Mater* 2000;**12**:2763–9.
27. Gaudon M, Apheceixborde A, Ménétrier M, Le Nestour A, Demourgues A. Synthesis temperature effect on the structural features and optical absorption of $Zn_{1-x}Co_xAl_2O_4$ oxides. *Inorg Chem* 2009;**48**:9085–91.
28. Ahmed IS, Shama SA, Dessouki HA, Ali AA. Low temperature combustion synthesis of $Co_xMg_{1-x}Al_2O_4$ nano pigments using oxalyldihydrazide as a fuel. *Mater Chem Phys* 2011;**25**:326–33.
29. Eppler R, Eppler D. Glazes and Glass Coating, The American Ceramic Society. Westerville, Ohio; 2000.
30. Keppler H, Bagdassarov N. The speciation of Ni and Co in silicate melts from optical absorption spectra to 1500 °C. *Chem Geol* 1999;**158**:105–15.
31. Costa G, Ribeiro MJ, Labrincha JA, Dondi M, Matteucci F, Cruciani G. Malayaite ceramic pigments prepared with galvanic sludge as colouring agent. *Dyes Pigments* 2008;**78**:157–64.
32. Hajjaji W, Zanelli C, Seabra MP, Dondi M, Labrincha JA. Cr-doped titanite pigment based on industrial rejects. *Chem Eng J* 2010;**158**:167–72.
33. DeVries RC, Roy R, Osborn EF. Phase equilibria in the system $CaO–TiO_2–SiO_2$. *J Am Ceram Soc* 1954;**38**:158–71.
34. DeCapitani C, Kirschen M. A generalized multicomponent excess function with application to immiscible liquids in the system $CaO–SiO_2–TiO_2$. *Geochim Cosmochim Acta* 1998;**62**:3753–63.
35. Abe S, Yamane H, Yoshida H. Synthesis and photoluminescence of Ca–(Sn,Ti)–Si–O compounds. *Mater Res Bull* 2010;**45**:367–72.
36. Stoyanova Lyubenova T, Matteucci F, Costa AL, Dondi M, Ocaña M, Carda J. Synthesis of Cr-doped $CaTiSiO_5$ ceramic pigments by spray drying. *Mater Res Bull* 2009;**44**:918–24.
37. Altunlu B, Ogut AZ, Toledo OD, Brett NH. Phase equilibria and microstructure in the systems $MgO–CaTiO_3$–calcium silicates. I. Isothermal sections within the systems $MgO–CaTiO_3–CaO·SiO_2$, $MgO–CaOTiO_3–2CaO·SiO_2$ and $MgO–CaTiO_3–3CaO·SiO_2$. *Br Ceram Trans J* 1984;**83**:83–8.
38. Lee Hyun-Soo, Lee Byung-Ha. Synthesis of sphene ($CaSnSiO_5$)-pink pigments with $CrCl_3$. *J Korean Ceram Soc* 2009;**46**:405–12.
39. Nakada H, Nagata K. Crystallization of $CaO–SiO_2–TiO_2$ slag as a candidate for fluorine free mold flux. *ISIJ International* 2006;**46**:441–9.
40. Grabner L, Stokowski SE, Brower Jr WS. No-Phonon $^4T_2g–^4A_2g$ Transitions of Cr^{3+} in TiO_2. *Phys Rev B* 1970;**2**:590–7.
41. Pavlov RS, Marza VB, Carda JB. Electronic absorption spectroscopy and color of chromium-doped solids. *J Mater Chem* 2002;**12**: 2825–32.
42. Vieira FTG, Souza SC, Oliveira ALM, Lima SLG, Longo E, Paskocimas CA, et al. Thermogravimetric and UV–vis spectroscopic studies of chromium redox reactions in rutile pigments. *J Therm Anal Calorim* 2009;**97**, 99-10.
43. Dondi M, Cruciani G, Guarini G, Matteucci F, Raimondo M. The role of counterions (Mo, Nb, Sb, W) in Cr-, Mn- Ni- and V-doped rutile ceramic pigments. Part 2. Colour and technological properties. *Ceram Int* 2006;**32**:393–405.